Available online at www.sciencedirect.com
ScienceDirect
Trans. Nonferrous Met. Soc. China 30(2020) 318−332
Transactions of Nonferrous Metals Society of China
www.tnmsc.cn

Hot cracking tendency test and simulation of 7075 semi-solid aluminium alloy

Bing ZHOU, Shuai LU, Kai-le XU, Chun XU, Zhan-yong WANG, Bin-jun WANG

School of Materials Science and Engineering, Shanghai Institute of Technology, Shanghai 201418, China

Received 23 February 2019; accepted 18 December 2019

Abstract: The hot cracking tendency of 7075 semi-solid alloy under different conditions was studied by critical diameter method. The experiment and simulation results show that the dendrite arms of the rod grow from the edge to the center. The smaller the diameter of the rod is, the more obvious the directional growth of dendrite is, and the greater the tendency of hot cracking is. Compared with ordinary melt, for semi-solid slurry, increasing mould temperature or decreasing pouring temperature can significantly decrease hot cracking tendency of 7075 alloy, decreasing hot cracking grade from 256 to 100 mm^2. Furthermore, based on the RDG criterion, the effects of solidification conditions on the hot cracking tendency were discussed combined with simulation. At the same time, the application and development of RDG criterion were also researched.

Key words: hot cracking tendency; semi-solid slurry; 7075 aluminium alloy; RDG criterion; numerical simulation

1 Introduction

Hot cracking is one of the most common and serious solidification defects in the casting process of 7xxx alloy [1−3]. It is the necessary and significant task to study the hot cracking properties. It occurs mainly in the later stage of solidification. The formation of hot cracking is related to many factors such as alloy composition, casting process, casting shape, mold condition and so on. Up to now, the hot tearing phenomenon has been studied extensively and deeply by researchers [4−8].

The evaluation method of hot cracking is mainly experimental testing method. ESKIN and SUYITNO [9] have listed several methods for assessing hot cracking tendency in the review, which are useful to analyze the grades of hot cracking during experiments. The mainstream evaluation methods are hot cracking ring method and the critical size method. The critical size method can be divided into the critical diameter method and the critical length method. TAGHIABADI et al [10] used the critical length method to study the effect of Cu on hot cracking tendency of A356 alloy. WANG et al [11] used a constrained rod casting apparatus (critical length method), equipped with a load sensor and a data acquisition system to study the effect of Cu content on the hot cracking behavior of the Mg−7Zn−*x*Cu−0.6Zr alloys. The critical diameter method was used to test the susceptibility coefficient of hot cracking alloys. In this method, the square of critical diameter of hot crack is taken as the evaluation index of hot cracking susceptibility coefficient. The larger the value is, the greater the hot cracking susceptibility is.

Semi-solid metal forming (SSF) is a kind of metal forming based on the good rheological properties of the metal in the semi-solid region during the transition of metal from solid to liquid or from liquid to solid. The semi-solid slurry has the

Foundation item: Project (17YF1407100) supported by the Shanghai Sailing Program of China; Project (17PJ1408600) supported by Shanghai Pujiang Program of China
Corresponding author: Bing ZHOU; Tel: +86-13248121983; E-mail: zb521a@sina.com
DOI: 10.1016/S1003-6326(20)65215-3

unique advantages of fine grain size and small shrinkage. The grain refinement can obviously improve the hot cracking tendency of the aluminum alloy [12,13]. At the same time, from the point of view of thermal cracking principle, solidification shrinkage is also helpful to reduce the tendency of thermal cracking. To the best of reducing the hot cracking in the casting process, 7075 semi-solid aluminium alloy was used to test and simulate in this work.

2 Experimental

2.1 Experimental method

In this work, the critical diameter method was used to evaluate the tendency of hot cracking of 7075 aluminium alloy. The principle of the method is as follows: The length of the test rods with different diameters is the same when these rods are injected to the hot cracking mould and the linear shrinkage is basically same too in this period. The difference of the deformation velocity and the effective bearing areas are due to the test rods with different diameters. Thin rods tend to hot-crack more easily than thick rods due to the fast cooling rate, fast deformation rate, small cross-sectional area and high stress of thin rods. In the case of other conditions being the same, the hot cracking grade of these samples is the square of the maximum diameter of the hot crack found. The higher the value of hot cracking grade is, the greater the tendency of hot cracking is and the poor the hot cracking resistance is.

Figure 1 shows the detailed size drawing of the mould for hot cracking with critical diameter method. In order to control the temperature of the mould, a heating sleeve with dimensions of 400 mm × 300 mm was added outside the mold. At the same time, temperature control box and the heating wire with power of 4 kW were used to heat and control the temperature of insulation device. The bottom of the insulation device was refractory cotton to insulate, and the mould was placed at the center of the insulation device.

The self-matched 7075 aluminum alloy ingot raw material was adopted in the experiment. The chemical composition is shown in Table 1. Through differential thermal scanning analysis of 7075 aluminum alloy used in the experiment, the solidus and liquidus temperatures of 7075 aluminum alloy were determined to be 477 and 640 °C, respectively. The whole process is as follows: Firstly, the liquid metal will be let stand and insulated after the ingot of 7075 aluminium alloy is dried, melted, refined, degassed, and the slag is discharged. Secondly, a certain amount of 7075 aluminium alloy liquid is obtained by using the spoon when the metal mould is preheated to a specified temperature. Thirdly, the 7075 aluminium alloy liquid is not poured into the hot cracking mould of the insulation until the temperature falls down to the set goal that the thermocouple measures. Other parameters of the process are the barrel temperature of 580−610 °C, the rotational speed of 300 r/min and the mixing time of 30 s. When the temperature thermocouple measured falls down to 640 °C, a certain amount of 7075 aluminium alloy liquid gained by using the spoon is

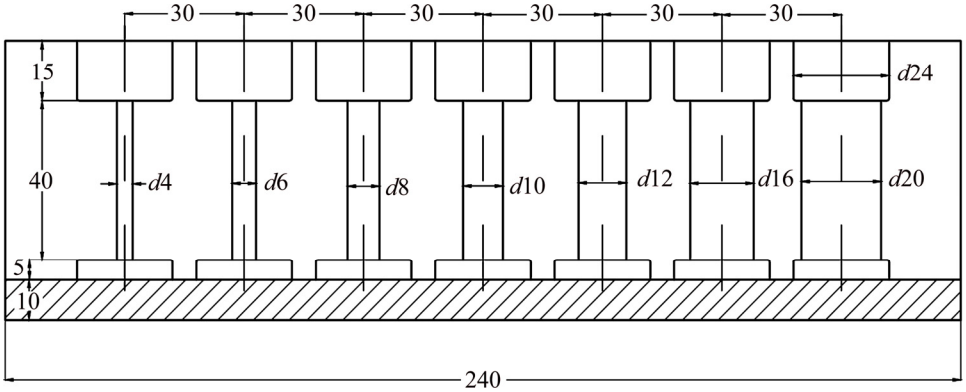

Fig. 1 Actual sizes of hot cracking mould for critical diameter method (unit: mm)

Table 1 Chemical composition of 7075 aluminum alloy (wt.%)

Zn	Mg	Cu	Cr	Fe	Mn	Si	Al
5.80	2.41	1.62	0.23	0.2	0.01	0.12	Bal.

poured into the forced convection semi-solid slurry preparation equipment [14,15], because the alloy solution makes forced convection in the stirring chamber. So, the temperature of the melt alloy decreases gradually. At this period, primary particles are abundant in nucleation. After stirring for a certain time, the alloy melt flowing from outlet to spoon is poured into the mould with the insulation device immediately. Finally, the sample in the mould is taken out after cooling down. Figure 2(a) shows the experimental diagram of hot cracking tendency during pouring. Figure 2(b) shows the mould with critical diameter method and the physical drawing of hot cracking test rods. The cross-section taken at the middle position of the upper test rod with different parameters is observed after grinding, polishing and eroding.

2.2 Mathematical models for simulation

2.2.1 Temperature field

The temperature field can be solved by the partial differential equation of Fourier heat conduction law, that is:

$$\rho c\frac{\partial T}{\partial t}=\frac{\partial}{\partial x}\left(\lambda_x\frac{\partial T}{\partial x}\right)+\frac{\partial}{\partial y}\left(\lambda_y\frac{\partial T}{\partial y}\right)+\frac{\partial}{\partial z}\left(\lambda_z\frac{\partial T}{\partial z}\right)+Q_{\mathrm{L}} \tag{1}$$

where ρ is the material density; c is the specific heat capacity; $T=(x,y,z,t)$ is the temperature; λ_x, λ_y and λ_z are heat conduction coefficients in directions of x, y and z, respectively; Q_{L} is the latent heat of crystallization.

The values of λ_x, λ_y, λ_z, ρ and c are related to temperature T. In order to simplify the calculation, only the case of $\lambda_x=\lambda_y=\lambda_z=\lambda$ is considered. At this point, the formula can be written as

$$\rho c\frac{\partial T}{\partial t}=\lambda\left(\frac{\partial^2 T}{\partial^2 x}+\frac{\partial^2 T}{\partial^2 y}+\frac{\partial^2 T}{\partial^2 z}\right)+Q_{\mathrm{L}} \tag{2}$$

According to different cases, Formulae (1) and (2) can give the following four kinds of boundary conditions.

(1) The first kind of boundary condition. The temperature T_{w} is determined to be a constant:

$$T_{\mathrm{w}}=f(x,y,z,t) \tag{3}$$

(2) The second kind of boundary condition. Heat flux can be determined as a constant:

$$q_{\mathrm{w}}=-\lambda\left(\frac{\partial T}{\partial n}\right)\Big|_{\mathrm{w}}=f(x,y,z,t) \tag{4}$$

where n is the outer normal direction of the object boundary, and the same as the heat flux.

(3) The third kind of boundary condition. The interfacial heat transfer coefficient h_{c} and the temperature of the surrounding fluid T_{f} can be determined as constant values:

$$-\lambda\left(\frac{\partial T}{\partial n}\right)\Big|_{\mathrm{w}}=h_{\mathrm{c}}\left(T_{\mathrm{w}}-T_{\mathrm{f}}\right) \tag{5}$$

(4) The fourth kind of boundary condition. In casting process, the thermal radiation on the surface of the casting can be expressed as

$$-\lambda\left(\frac{\partial T}{\partial n}\right)\Big|_{\mathrm{w}}=\varepsilon'\sigma'\left(T_{\mathrm{w}}^4-T_{\mathrm{f}}^4\right) \tag{6}$$

where σ' is the Stefan−Boltzmann constant; ε' is the emissivity. Among the former conditions, the first is the forced boundary condition, the second and the third are the natural boundary conditions.

2.2.2 Flow field

In the numerical simulation of the filling process, the flow of liquid metal obeys the law of fluid dynamics, and the most widely used mathematical model is the method of SOLA-VOF [16].

Fig. 2 Experimental diagram of hot cracking tendency (a) and hot cracking mould and test rod (b)

(1) Continuity equation

$$\frac{\partial u}{\partial x}+\frac{\partial v}{\partial y}+\frac{\partial w}{\partial z}=0 \tag{7}$$

where u, v and w are velocity components in x, y and z directions, respectively.

(2) N−S Equation

$$\rho\left(\frac{\partial u}{\partial t}+u\frac{\partial u}{\partial x}+v\frac{\partial u}{\partial y}+w\frac{\partial u}{\partial z}\right)=-\frac{\partial p}{\partial x}+\rho g_x+\mu\nabla^2 u \tag{8}$$

$$\rho\left(\frac{\partial v}{\partial t}+u\frac{\partial v}{\partial x}+v\frac{\partial v}{\partial y}+w\frac{\partial v}{\partial z}\right)=-\frac{\partial p}{\partial y}+\rho g_y+\mu\nabla^2 v \tag{9}$$

$$\rho\left(\frac{\partial w}{\partial t}+u\frac{\partial w}{\partial x}+v\frac{\partial w}{\partial y}+w\frac{\partial w}{\partial z}\right)=-\frac{\partial p}{\partial z}+\rho g_z+\mu\nabla^2 w \tag{10}$$

where p is the fluid pressure; g is the gravitational acceleration; μ is the viscosity of the fluid.

(3) Energy equation

$$\rho c\left(\frac{\partial T}{\partial t}+u\frac{\partial T}{\partial x}+v\frac{\partial T}{\partial y}+w\frac{\partial T}{\partial z}\right)= k\frac{\partial}{\partial x}\left(\frac{\partial T}{\partial x}\right)+k\frac{\partial}{\partial y}\left(\frac{\partial T}{\partial y}\right)+k\frac{\partial}{\partial z}\left(\frac{\partial T}{\partial z}\right)+S \tag{11}$$

where S is the source term.

The heat conduction process consists of two parts, the thermal conductivity of the fluid and the heat transferred by its macroscopic displacement.

2.2.3 Stress field

There are three stages in the solidification process of castings: liquid, two-phase zone and solid. When the casting is in the molten state, the temperature field has no effect on the distribution of the force field. When the casting is in the two-phase zone or solid state, the small change in temperature will cause a large change in stress. In the casting process, the heat dissipation from the casting to the outside and the cooling water effect on the casting make the temperature distribution in the casting uneven, which finally leads to the generation of thermal stress. At the same time, part of the deformation work produced by the thermal stress is transformed into heat, which affects the temperature field.

In elasticity, the relationship between stress and strain is

$$\{\sigma\}=[\boldsymbol{D}_e]\{\varepsilon_e\} \tag{12}$$

where $\{\sigma\}$ is the elastic stress; $\{\varepsilon_e\}$ represents the elastic strain; $[\boldsymbol{D}_e]$ is the elastic modulus matrix and can be expressed as

$$[\boldsymbol{D}_e]=\frac{E(1-\nu)}{(1+\nu)(1-2\nu)}\cdot\begin{bmatrix} 1 & \frac{\nu}{1-\nu} & \frac{\nu}{1-\nu} & 0 & 0 & 0 \\ & 1 & \frac{\nu}{1-\nu} & 0 & 0 & 0 \\ & & 1 & 0 & 0 & 0 \\ & & & \frac{1-2\nu}{2(1-\nu)} & 0 & 0 \\ & \text{Symmetry} & & & \frac{1-2\nu}{2(1-\nu)} & 0 \\ & & & & & \frac{1-2\nu}{2(1-\nu)} \end{bmatrix} \tag{13}$$

where E is the elastic modulus; ν is the Poisson ratio. The relationship between strain and displacement is

$$\{\varepsilon\}=[\boldsymbol{B}]\{\delta\} \tag{14}$$

where $\{\delta\}$ is nodal displacement array; $[\boldsymbol{B}]$ is strain−displacement matrix. $[\boldsymbol{B}]$ can be expressed as

$$[\boldsymbol{B}]=\begin{bmatrix} \frac{\partial}{\partial x} & 0 & 0 \\ 0 & \frac{\partial}{\partial y} & 0 \\ 0 & 0 & \frac{\partial}{\partial z} \\ \frac{\partial}{\partial y} & \frac{\partial}{\partial x} & 0 \\ 0 & \frac{\partial}{\partial z} & \frac{\partial}{\partial y} \\ \frac{\partial}{\partial z} & 0 & \frac{\partial}{\partial x} \end{bmatrix} \tag{15}$$

So the relationship between stress and displacement is

$$\{\sigma\}=[\boldsymbol{D}_e][\boldsymbol{B}]\{\varepsilon_e\} \tag{16}$$

Effective stresses are often used to determine whether a material is in the yield range, which are expressed as

$$\bar{\sigma}=\frac{\sqrt{3}}{2}\sqrt{(\sigma_1-\sigma_2)^2+(\sigma_2-\sigma_3)^2+(\sigma_3-\sigma_1)^2} \tag{17}$$

$$\bar{\sigma}=\frac{\sqrt{3}}{2}[(\sigma_{xx}-\sigma_{yy})^2+(\sigma_{yy}-\sigma_{zz})^2+(\sigma_{zz}-\sigma_{xx})^2+6(\sigma_{xy}^2+\sigma_{yz}^2+\sigma_{zx}^2)]^{1/2} \tag{18}$$

where $\bar{\sigma}$ is the average stress; σ_1, σ_2 and σ_3 are the three principal stresses; σ_{xx}, σ_{yy} and σ_{zz} are the normal stresses in directions of x, y and z, respectively; σ_{xy}, σ_{yz} and σ_{zx} are the shear stresses.

In the same way, the equivalent strain effect is

$$\bar{\varepsilon}=\frac{\sqrt{3}}{2}\sqrt{(\varepsilon_1-\varepsilon_2)^2+(\varepsilon_2-\varepsilon_3)^2+(\varepsilon_3-\varepsilon_1)^2} \tag{19}$$

$$\bar{\varepsilon}=\frac{\sqrt{3}}{2}[(\varepsilon_{xx}-\varepsilon_{yy})^2+(\varepsilon_{yy}-\varepsilon_{zz})^2+(\varepsilon_{zz}-\varepsilon_{xx})^2+\frac{3}{2}(\varepsilon_{xy}^2+\varepsilon_{yz}^2+\varepsilon_{zx}^2)]^{1/2} \tag{20}$$

where ε_1, ε_2 and ε_3 are the three principal strains; ε_{xx}, ε_{yy} and ε_{zz} are the normal strains in directions of x, y and z, respectively; ε_{xy}, ε_{yz} and ε_{zx} are the shear strains.

The plastic treatment in the thermal elasto-plastic model is quite complicated. The plastic stress−strain relation theory is mainly divided into the deformation theory and the flow theory. For the elastic model, the stress and strain increment can be expressed as

$$\{\mathrm{d}\varepsilon_\mathrm{T}\}=[\boldsymbol{D}_\mathrm{e}]\{\mathrm{d}\varepsilon_\mathrm{e}\} \tag{21}$$

$$\{\mathrm{d}\varepsilon_\mathrm{T}\}=\left(\{\alpha\}\,\mathrm{d}T+(T-T_0)\frac{\partial\{\alpha\}}{\partial T}+\frac{\partial[\boldsymbol{D}_\mathrm{e}]^{-1}}{\partial T}\{\sigma\}\right) \tag{22}$$

where ε_T is the thermal strain; $\{\alpha\}$ is the coefficient of thermal expansion.

The total strain includes elastic strain and thermal strain. The formula is expressed as

$$\{\mathrm{d}\varepsilon\}=\{\mathrm{d}\varepsilon_\mathrm{e}\}+\{\mathrm{d}\varepsilon_\mathrm{T}\} \tag{23}$$

3 Results

3.1 Effect of mould temperature

Besides the *d*20 mm, the test rod has the thermal crack under the parameters of the mould temperature of 25 °C (room temperature) and the solution temperature of 670 °C. Figure 3 shows the metallographic photographs of hot cracking test rods with different diameters. The microstructure of the hot cracking test rod of ordinary melt is mainly

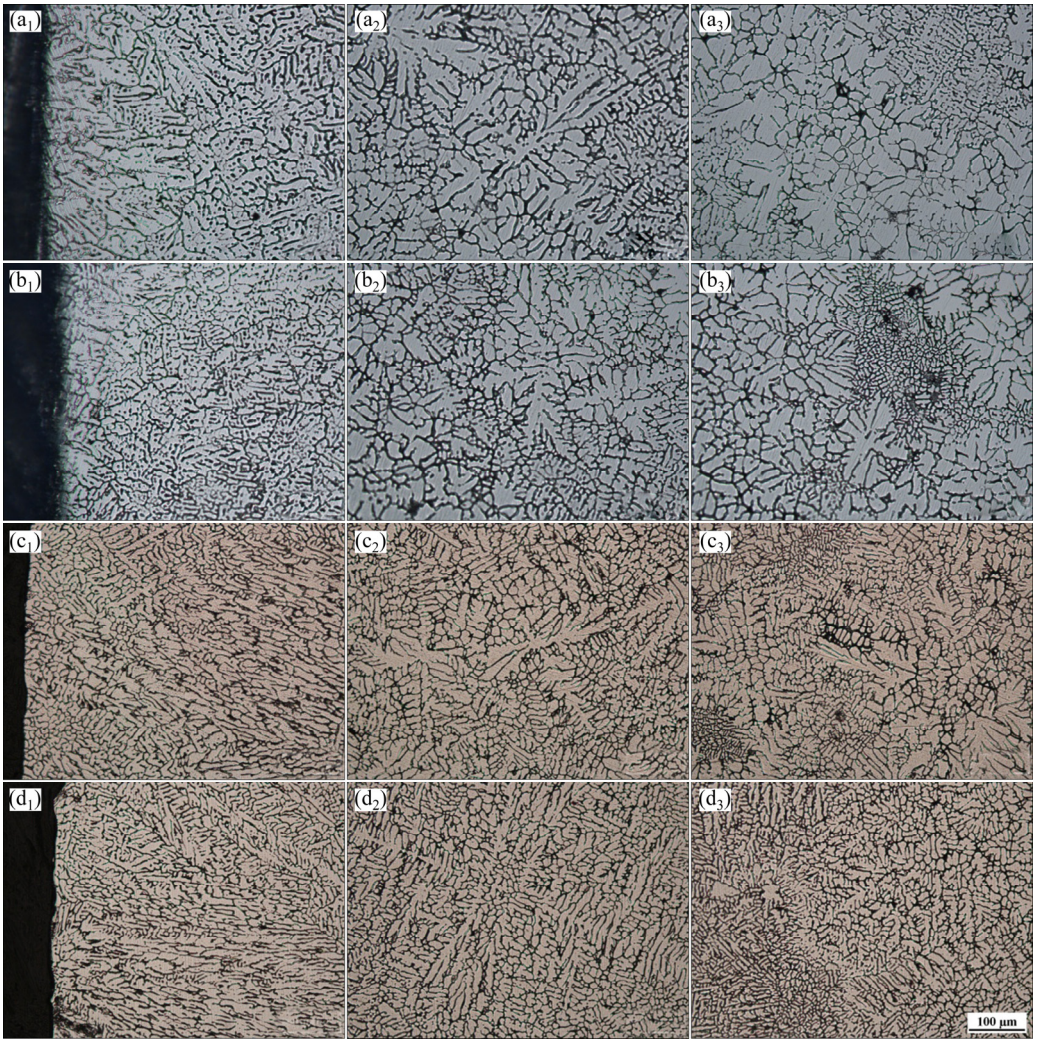

Fig. 3 Microstructures of hot cracking test rods with different diameters under mould temperature of 25 °C (room temperature): (a) 20 mm; (b) 16 mm; (c) 12 mm; (d) 10 mm; 1—Edge; 2—Middle; 3—Center

composed of dendrites, the size of which is 200−500 μm. According to the comparison from edge to center in Fig. 3, dendrites near the edge wall grow towards the center, the middle dendrite arm develops well, and the dendrite arm at the center is larger. It can be seen from Fig. 3 that, the smaller the diameters are, the longer the dendrite arms of all dendrites are, and the more obvious the direction of dendrite growth on the edges is, which will increase the tendency of hot cracking.

In order to compare the hot cracking properties of semi-solid slurry and common melt at different mould temperatures, the hot cracking test rod of ordinary melt at 650 °C was studied firstly. A very large tendency of hot cracking occurred in aluminium alloy when the melt with a temperature of 650 °C was poured into the hot cracking mold under the situation of heat insulation. All other test rods broke except the hot cracking test rod with the maximum diameter. Furthermore, the hot cracking grade of the test rod is 256 mm^2. It is found that at the mould temperatures of 25, 130 and 230 °C, the *d*20 mm rods were not cracked and the *d*16 mm rods were all fractured at the same hot cracking grade. Figure 4 shows the hot cracking rods of 16 mm poured with ordinary slurry at different mould temperatures. The hot cracking tendency of 7075 aluminum alloy is very large and the hot cracking grade cannot be obviously reduced by increasing the mould temperature, but it can be seen from Fig. 4 that the hot cracking degree of the test rod has been reduced to some extent.

Figure 5 shows the hot cracking test rod poured with semi-solid slurry at different mould temperatures. The technological parameter of semi-solid slurry preparation is pouring temperature of 650 °C. After the preparation of semi-solid slurry, it was directly poured into hot cracking mould. It can be seen from Fig. 5(c) that there is no crack on the *d*20 mm rod cast by semi-solid slurry at room temperature. There were slight surface cracks near the upper part of the *d*16 mm rod and obvious cracks appeared on the *d*12 mm rod. Furthermore, cracks can be seen obviously on the *d*10 mm rod. When the mould temperature increased to 130 °C, there were no crack lines on *d*20 mm and *d*16 mm rods while the *d*12 mm and *d*10 mm rods obviously cracked. When the mould temperature increased to 230 °C, there were no cracks on the rods of *d*20 mm, *d*16 mm and 12 mm. But the *d*10 mm rods obviously cracked.

Figure 6 shows the comparison of hot cracking grades (areas) between ordinary slurry and semi-solid slurry casting at different mould temperatures.

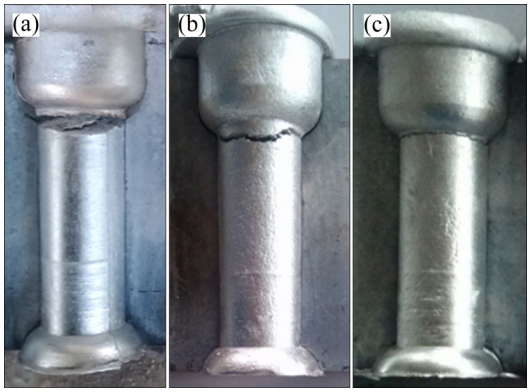

Fig. 4 Hot cracking test rods with diameter of 16 mm poured with ordinary slurry at different mould temperatures: (a) 25 °C; (b) 130 °C; (c) 230 °C

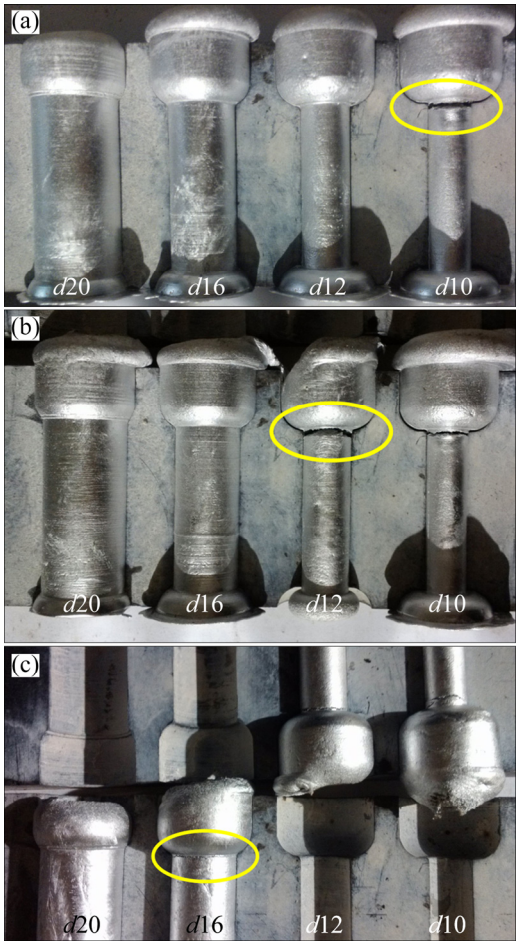

Fig. 5 Hot cracking test rods poured with semi-solid slurry at different mould temperatures (unit: mm): (a) 230 °C; (b) 130 °C; (c) 25 °C

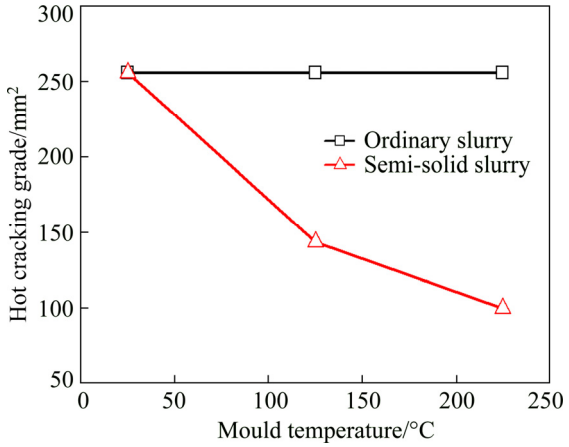

Fig. 6 Hot cracking grades of ordinary and semi-solid slurries at different mould temperatures

It is found that the hot cracking grades of semi-solid alloy slurry are all lower than those of common slurry at the same mould temperature. Furthermore, the hot cracking tendency of semi-solid slurry can be obviously reduced by increasing the mould temperature. When the mould temperature is 230 °C, the hot cracking grade of semi-solid slurry is 100 mm^2.

Figure 7 shows the microstructures of *d*12 mm hot cracking rods at different positions under the condition of different mould temperatures with the mould cooling. At different mould temperatures, the semi-solid structure can be found in the edge, middle and center of the semi-solid hot cracking test rod. However, the higher the mould temperature is, the less the number of dendrites and the more spherical the morphology of the grains is. The dendrite structure of the hot cracking rods is obviously different from that of the ordinary rods. The microstructure of semi-solid slurry test rod is mostly composed of near-spherical and small dendrites, and its size is 50−100 μm. Under the condition of mould with room temperature, the temperature of the slurry decreases rapidly and the temperature gradient is large. When the mould temperature is raised to 130 °C, the temperature of semi-solid slurry and the temperature gradient decrease. The dendrite shape and appearance are improved and the grain size is refined. When the mould temperature increases to 230 °C, the temperature of semi-solid slurry decreases more slowly. The temperature gradient is smaller and the

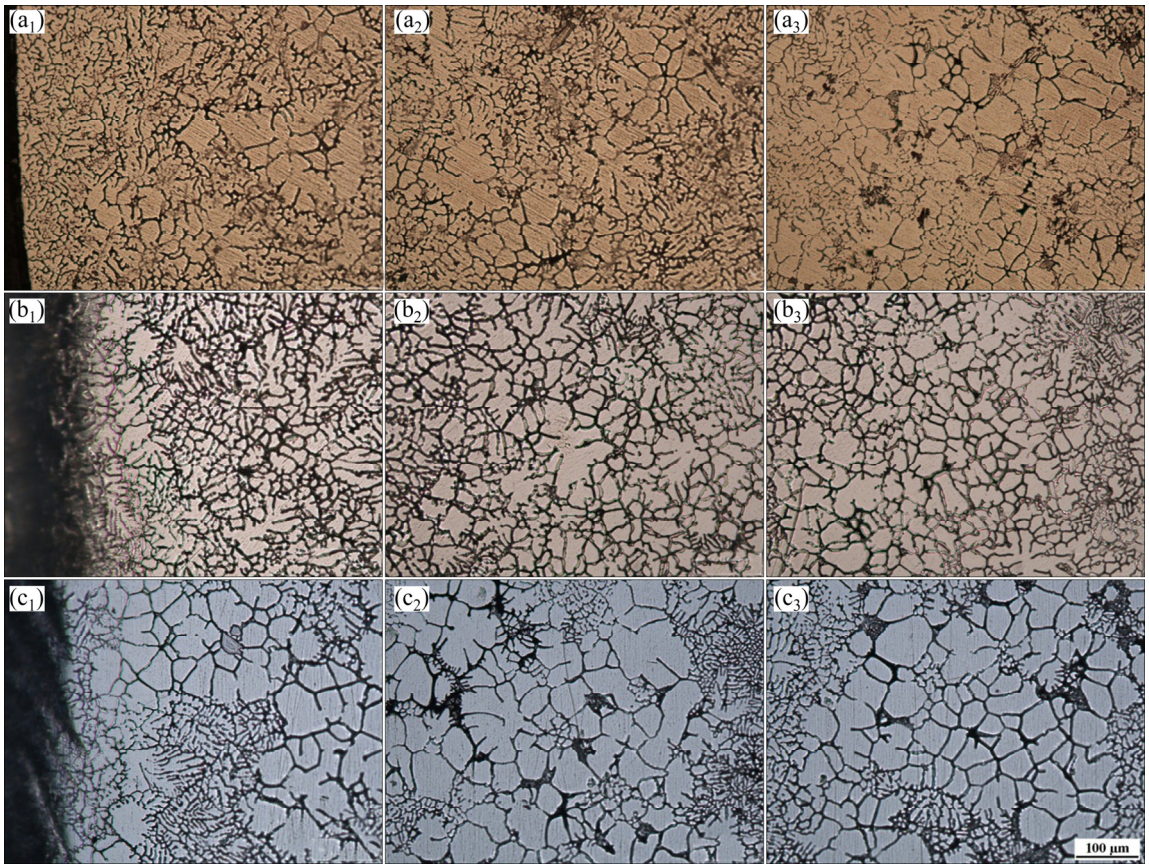

Fig. 7 Microstructures of semi-solid aluminum alloy at different positions of *d*12 mm test rods and different mould temperatures: (a) 25 °C; (b) 130 °C; (c) 230 °C; 1—Edge; 2—Middle; 3—Center

number of small dendrites in the edge is obviously reduced. At the same time, the morphology of the edge, middle and center is obviously improved. Compared with room temperature and 130 °C, the dendrites at mould temperature of 230 °C have been refined and improved obviously.

3.2 Effect of pouring temperature

In order to compare the hot cracking properties of semi-solid slurry and common melt at different pouring temperatures, the properties of hot cracking test rods with pouring temperatures of 690, 670 and 650 °C and mould temperature of 230 °C were studied. It is found that no cracks are found in the *d*20 mm rods at three different pouring temperatures and all the *d*16 mm rods are fractured. They are all in the same hot cracking grade.

Figure 8 shows the physical diagrams of hot cracking test rods poured with semi-solid slurry at different pouring temperatures. The mould temperature is 230 °C. When pouring temperature is 690 °C, there are no cracks in *d*20 mm test rod but there are small cracks in upper part of *d*16 mm rod. When pouring temperature is 670 °C, there are no cracks in *d*20 mm and *d*16 mm test rods but there are obvious cracks in *d*12 mm test rods. When the pouring temperature is 650 °C, the real experimental test rods are shown in Fig. 5(a), other parameters are the same. The result shows that there are no cracks in *d*20 mm, *d*16 mm and *d*12 mm test rods but there are some cracks in *d*10 mm test rods.

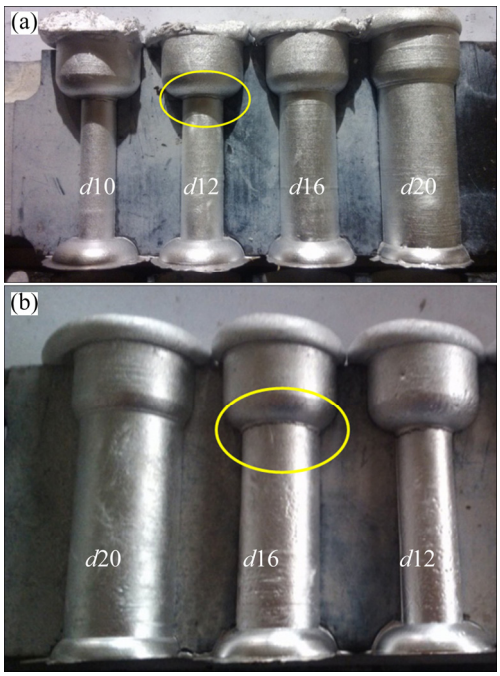

Fig. 8 Hot cracking test rods poured with semi-solid slurry at pouring temperatures of 670 °C (a) and 690 °C (b) (unit: mm)

Figure 9 shows a comparison of the hot cracking grades of the common slurry and the semi-solid slurry at different pouring temperatures. It is found that for the common slurry even at the higher mould temperature, the hot cracking tendency of 7075 aluminum alloy cannot be effectively reduced by lowering the pouring temperature. For semi-solid slurry, the hot cracking tendency of 7075 aluminum alloy can be effectively reduced by lowering the pouring temperature. The hot cracking area of semi−solid slurry prepared under the pouring temperature of 650 °C is 100 mm^2.

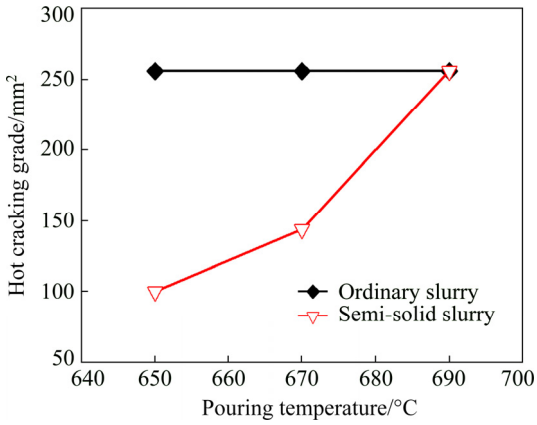

Fig. 9 Hot cracking grades of rods with common slurry and semisolid slurry at different pouring temperatures

Figure 10 shows the microstructures of *d*12 mm hot cracking rod of different positions at different pouring temperatures with the cooling of mould. The mould temperature is 230 °C. At different pouring temperatures, the microstructure of the alloy is obviously different from that of the hot cracking rod. When the pouring temperature is decreased, the structures of the edge, middle and center are obviously improved and the tendency of hot cracking is also reduced. With the further lowering of pouring temperature in the process, the grains ranging from rose-shaped to nearly spherical in the semi-solid structure become finer, more numerous and more spherical, as shown in Fig. 10(c).

3.3 Hot cracking tendency under different conditions

3.3.1 Hot cracking criterion

To analyze hot cracking tendency in casting,

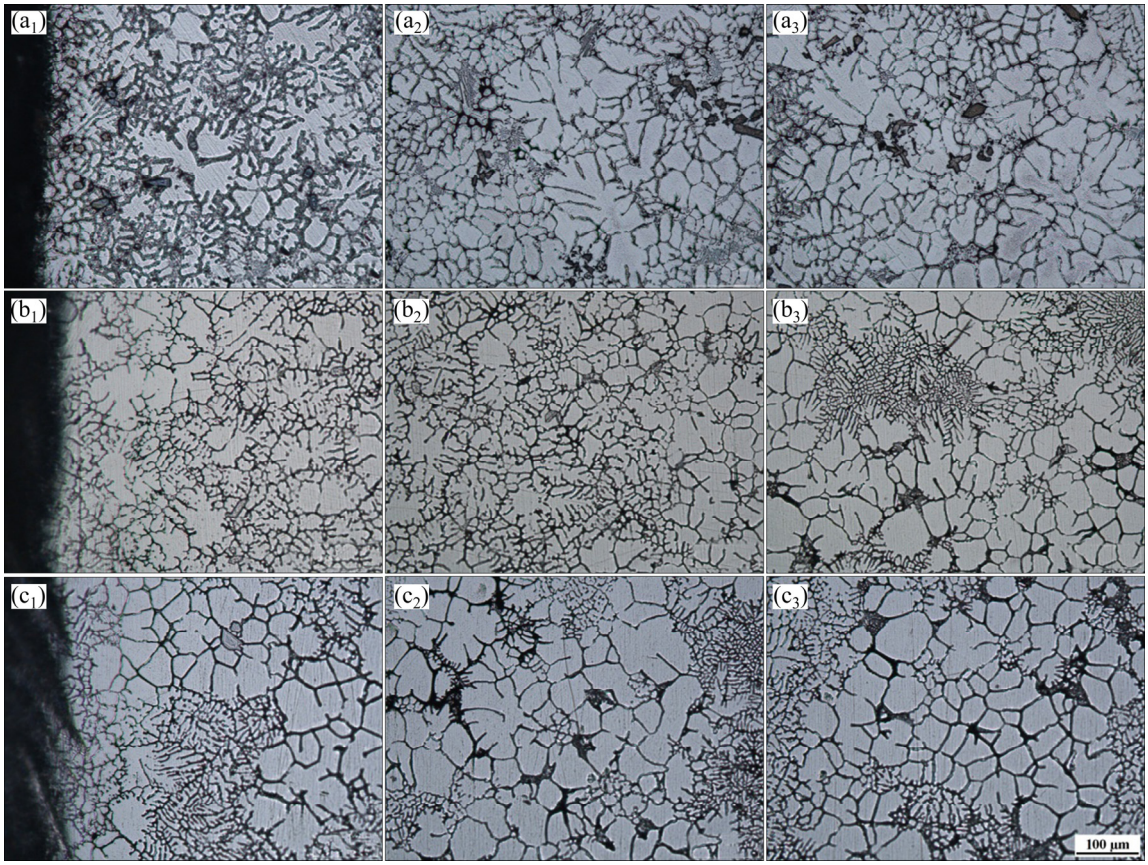

Fig. 10 Microstructures of *d*12 mm test rods poured with semi-solid slurry at different positions and different pouring temperatures: (a) 690 °C; (b) 670 °C; (c) 650 °C; 1—Edge; 2—Middle; 3—Center

several criteria have been developed. These criteria can be mainly divided into two categories: mechanical and non-mechanical. The mechanical criteria involve critical stress, critical strain and critical strain rate. The non-mechanical criteria normally deal with the temperature range, phase diagram and process parameters such as pouring temperature and mould temperature.

An overview of the hot cracking criterion derived by RAPPAZ et al [17] is called the RDG criterion. In this criterion, the dendrites are assumed to grow at a given thermal gradient (G) and with a velocity of V_T.

Considering that the fluid moves along the thermal gradient only, whereas the solid deforms in the transverse direction, one can calculate the pressure within the mush:

$$p=p_a+\rho gh-\Delta p_{sh}-\Delta p_{mec} \tag{24}$$

where p_a is the atmospheric pressure, ρgh is the metallostatic contribution, Δp_{sh} and Δp_{mec} are the pressure drop contributions in the mush associated with the solidification shrinkage and the deformation induced fluid flow, respectively. In steady state conditions and assuming a uniform mechanical deformation rate throughout the mush, these two contributions are given by

$$\Delta p_{sh}+\Delta p_{mec}=\frac{180\mu}{G\lambda^2}\left[V_T\beta A+\frac{(1+\beta)B\dot{\varepsilon}}{G}\right] \tag{25}$$

With $A=\int_{T_{cg}}^{T_{mf}}\frac{f_s^2\mathrm{d}T}{(1-f_s)^2}$, $B=\int_{T_{cg}}^{T_{mf}}\frac{f_sF_s(T)}{(1-f_s)^3}\mathrm{d}T$ and $F_s(T)=\int_{T_{cg}}^{T}f_s\mathrm{d}T$.

where T_{cg} is the coalescence temperature of dendrite arms and T_{mf} is the mass feeding temperature; λ is the mean grain size for equiaxed structures or the secondary dendrite arm spacing for columnar structures; β is the solidification shrinkage factor; f_s is the solid volume fraction. Two parameters A and B depend only on the nature of the alloy and its solidification path, i.e. on the relationship between f_s and T. Equation (25) reveals that the shrinkage contribution is proportional to the speed of the isotherms, whereas the mechanical contribution is proportional to the strain rate. Both contributions

are inversely proportional to the square of the grain size.

Eventually, if the pressure, p, given by Eqs. (24) and (25), falls below the cavitation pressure, p_c, a hot cracking forms. This condition allows the calculation of the maximum strain rate to be sustainable by the mushy zone, $\dot{\varepsilon}_{max}$, and a hot cracking susceptibility (HCS) reflecting hot cracking tendency, can be defined as $1/\dot{\varepsilon}_{max}$. The higher the HCS is, the more susceptible the alloy is.

3.3.2 Hot cracking tendency at different mould temperatures

The faster the rod solidifies, the larger the cooling rate is. Under the condition of the same linear shrinkage, the faster the shape changes, the greater the strain is. The comparison of effective plastic strain of hot cracking test rods with different sizes at different mould temperatures is shown in Fig. 11 (same model size with Fig. 1). At the same mould temperature, the effective plastic strain of the thin rod is larger than that of the coarse rod and the effective strain of the upper part of the thin rod is greater than that of the middle and lower part of the rod. With increasing the mould temperature from 25 to 230 °C, the effective plastic strain of hot cracking rod with the same size is obviously reduced.

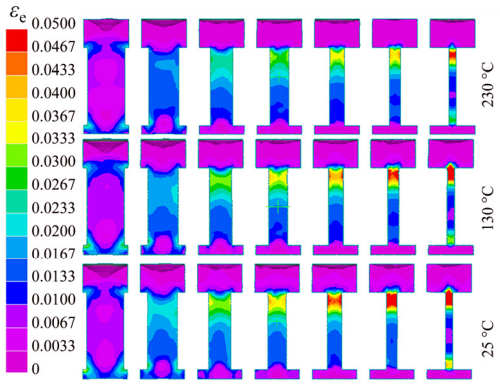

Fig. 11 Comparison of effective plastic strain (ε_e) of test rods at different mould temperatures

Figure 12 shows the comparison of hot cracking tendency of test rods with different sizes at different mould temperatures. At the same mould temperature, the hot cracking tendency of thin rod is higher than that of coarse rod, and hot cracking tendency of the upper part of the rod with larger size difference is obviously greater than that of the middle and lower parts. At the same time, the hot cracking tendency of the same size test rod decreases with the increase of mould temperature.

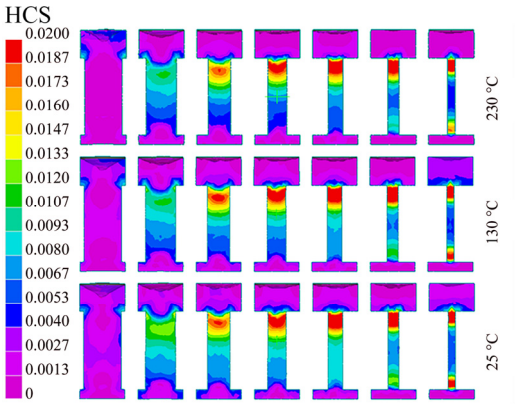

Fig. 12 Comparison of hot cracking tendency of test rods at different mould temperatures

3.3.3 Hot cracking tendency at different pouring temperatures

Figure 13 shows the comparison of the effective plastic strain of the hot cracking rod at pouring temperatures of 690, 670 and 650 °C. The mould temperature is 25 °C. The higher the pouring temperature is, the larger the temperature difference between the edge and the center is, which is not conducive to the uniform growth of grains in all directions. When the pouring temperature and mould temperature are not changed, the effective plastic strain increases with the decrease of the diameter of the rod. At the same mould temperature, the effective plastic strains of different sizes are reduced with the decrease of pouring temperature.

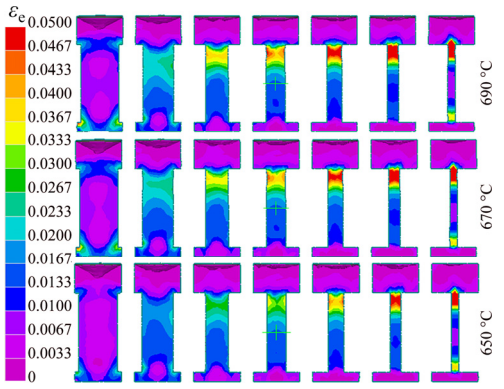

Fig. 13 Comparison of effective plastic strain of test rods at different pouring temperatures

Figure 14 shows the comparison of hot cracking susceptibility of rods with different sizes at different pouring temperatures. At the same pouring temperature and mould temperature, the hot cracking tendency of the thin rod is greater than that

of the thick rod. The hot cracking tendency of the middle and upper parts of the rod with large difference in size is obviously higher than that of the middle and lower parts and the hot cracking tendency of the same size rod decreases with the decrease of pouring temperature.

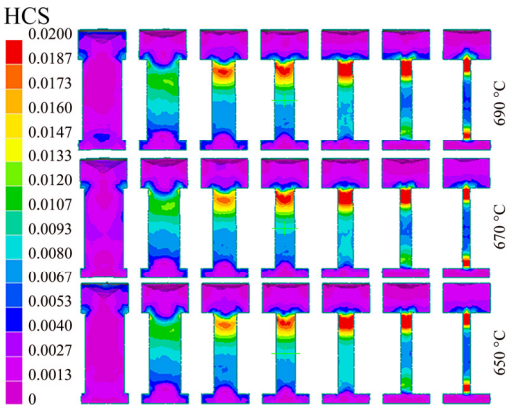

Fig. 14 Comparison of hot cracking tendency of test rods at different pouring temperatures

4 Discussion

4.1 Effect of solidification on hot cracking

In traditional solidification process, the melt near the cold wall of the mould firstly solidifies followed by the center with high level of alloying elements and impurity elements. According to the thermodynamics of metal solidification, supercooling is the driving force of solidification. When melt is poured into the mould with room temperature, a huge temperature difference will occur. This temperature difference is the supercooling. According to the dynamics of solidification, for homogeneous nucleation and heterogeneous nucleation, the critical nucleation radius is inversely proportional to the degree of supercooling and the critical nucleation energy varies inversely with the square of the degree of supercooling, so degree of supercooling is related to the nucleation. The difference will lead to different cooling rates among the grains. Under the circumstance of supercooling, some grains are survived and become the core of nucleation. The amount of the crystal nucleus survived is less and only the larger grains can exist. This is because some grains are melted by superheated temperature. Only a small amount of above grains exist in the solidification and the main microstructure is dendrites. Furthermore, the dendrites will grow up consistently towards the direction of cooling. After pouring into the mould, the structure near the edge wall grows rapidly and a large number of dendrites are formed. The large grains in the middle and the center grow up more often because of the slower cooling, which makes them easy to grow into the dendritic crystal with very large dendrite arms. The dendrites start to form a solid skeleton and the liquid flows throughout the dendrite networks. According to the solidification shrinkage compensation theory, the liquid flow is blocked and cannot proceed when the dendrites form a continuous network structure. During the process, due to the lack of space for the growth of different rates, these dendrites will compete with each other. The effective plastic strain is reflected from the competition of these dendrites. In a word, the strain can be affected by the mould temperatures. At the same time, the impurity and other elements solidify at last. They act as a stress concentration region in the microstructure, thus promoting the nucleation of hot tears. The whole process can be seen in Fig. 15. The phenomenon of “survival of the fittest” and different chemical compositions between dendrites and impurity resulting from the mould temperatures lead to the hot cracking.

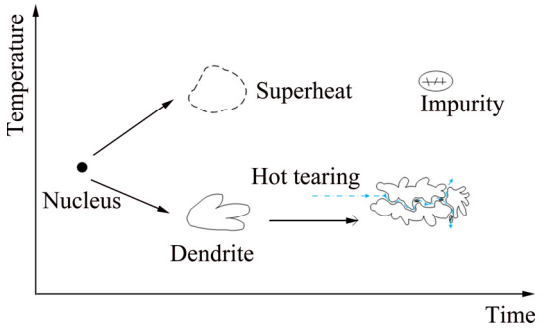

Fig. 15 Schematic diagram of traditional solidification and development of hot cracking

Compared with traditional solidification, the number of surviving crystal nuclei is increased during the semi-solid forming process. The solid phase in the semi-solid slurry is also increased and the number of grains is greatly increased. During the same period of solidification, except for the mould temperature, the microstructure of semi-solid slurry is also affected by pouring temperature. At the same period, a high casting temperature can increase the temperature gradients, which promotes the growth of columnar dendrites, as AKHYAR et al indicated [18]. The grains are relatively small

after pouring into the mould because of a large number of grains resulting from the temperature gradients. Due to the increase of mutual inhibition, cores in semi-solid slurry grow to approximately spherical grains because the temperature field of the melt becomes uniform and the environment for dendrite growth is destroyed. Furthermore, the new nucleation grains in the liquid phase are also difficult to grow into dendrites because of the influence of the surrounding grains. Grains of semi-solid aluminium alloy grow at a relatively balanced speed to make themselves more spherical during the solidification. Therefore, there is no intense competition between the grains. The effective plastic strain can be changed obviously by different pouring temperatures. The grades of hot cracking can be seen from the crack length on the surface of the test rods. BIRRU and KARUNAKAR [19] have indicated that the crack length of alloy, which appears normally in the process of solidification, can be greatly reduced at the minimum pouring temperature but is not completely prevented. So, lowering the pouring temperature can improve the nucleation environment in the solidification. It can make the grains finer, more spherical and uniform. At the same time, it increases more grain interfaces. More grain, interfaces mean smaller tendency of hot cracking because more grain boundaries are resistant to the strength from shrinkage. Under the same stress, it is difficult to make hot cracking. Therefore, the higher temperature leads to smaller solidification shrinkage, which can significantly reduce the hot cracking. The whole process can be seen from Fig. 16.

The influence of pouring temperature on hot cracking is similar to the mould temperature. The

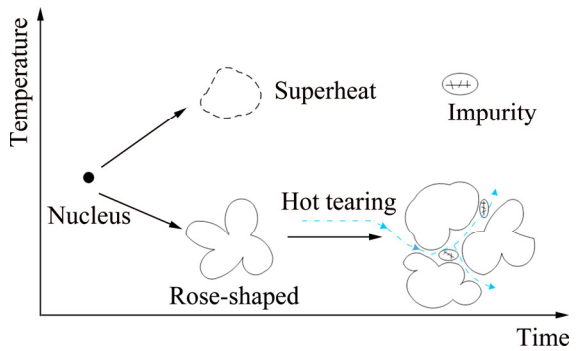

Fig. 16 Schematic diagram of semi-solid solidification and development of hot cracking

former is the external cause, but the latter is the internal cause of slurry.

4.2 Application and development based on RDG criterion

Hot cracking is the result of external or internal stress or both during the solidification and subsequent shrinkage near the solid line. According to Ref. [20], columnar dendritic grains growing in one direction are considered, with tensile deformation normal to the growth direction and liquid feeding opposite to the growth direction. According to the evaluation in Ref. [21], RDG criterion shows the greatest potential in the qualitatively prediction of HTS. The RDG model was used by BÖLLINGHAUS et al [22] to study the solidification cracking of some Al alloys. The HCS values under this criterion were calculated and compared with each other. CONIGLIO and CROSS [23] studied Al arc welds with the RDG model and a crack growth model was proposed to relate the crack growth rate to the local strain rate based on the RDG criterion. In Ref. [22], the RDG criterion was applied to the welding of aluminum alloys successfully.

Based on the criterion of RDG hot cracking combining with semi-solid slurry, some interesting rulers can be obtained.

On one hand, before the solidification, the grains have not coalesced yet and are free to move within the liquid. These grains present a state of irregular movement. There is no restriction between them. However, on the other hand, below the temperature at which coalescence of the grains takes place, all the grains form a coherent solid network which can transmit the thermal stress induced by cooling. The heat can be transferred from one to another between the grains through the network. At some parts of network, the transmission of heat cannot be conveyed uniformly. Due to the uneven distribution of heat, the growth directions of grains are also different. This will lead to the anisotropic phenomenon. The dendrites will grow along the direction of cooling. At the same time, dendrite arms of different dendrites intersect and overlap, showing a state of disorder without the law of motion. When different arms intersect with each other, heat flows through the network from other places to a junction. The heat of this junction is over the average temperature of the whole system.

At this time, the local hot spots appear from all over the network. This means that hot spots occur in the network dynamically. Due to the uneven distribution of temperature, the second undercooling will appear. The first and the second growth of dendrite arms can lead to the tendency of hot cracking more obviously.

In the range of solidification temperature, the theory of a thin film of liquid between dendrites was offered by ESKIN and SUYITNO [9]. The film of liquid can only resist up a cavitation pressure at which a void is nucleated. Solidification shrinkage induced a negative volume change in the alloys during the phase transformation. According to AKHYAR et al [18], pressure-feeding across dendrites is required to avoid the formation of hot tears. With further solidification, the film of liquid cannot compensate for shrinkage any more. It cannot develop into a hot tear until exceeding the tolerance of limit. When it is turned into the hot cracking, any opening of the continuous liquid film present in the slurry can hardly be compensated for by feeding from the upper region of the mush because of the high volume fraction of solid. When the opening cannot be given by continuous slurry, the macroscopic hot cracking is visible obviously.

Figure 17 shows a schematic diagram of the equiaxed dendritic growth in inoculated aluminum alloys. Above the mass feeding temperature, T_{mf}, the grains have not yet coalesced and are free to move within the liquid. However, below the temperature at which coalescence of the grains takes place, T_{cg}, all the grains form a network which can transmit the heat induced by cooling. Above a certain volume fraction of grains, mass feeding can no longer compensate for shrinkage, with the specific mass of the solid being larger than that of the liquid for most metallic alloys. Therefore, the liquid has to flow from the right to the left in a packed bed of solid grains. Combined with semi-solid forming, among all the required parameters, Δp is a key value. This condition can be rewritten in terms of depression:

$$\Delta p=p_a-p=\Delta p_{sh}+\Delta p_{mec}-\rho gh<\Delta p_c \quad (26)$$

where the cavitation depression is defined as $D_{pc}=p_a-p_c$.

Temperature takes control of the whole process of nucleation. During the solidification, supercooling occurs with the decrease of the temperature. It is the power source of the process from which nucleus can nucleate and grow. When the cores turn into dendrites or approximately spherical grains, the changes of stress between large amounts of grains result in the pressure. This pressure belongs to the internal stress of the melt. Because the atmosphere pressure belongs to the external stress, when this pressure of the melt falls below the atmosphere pressure, the condition is conductive to the generation of hot cracking.

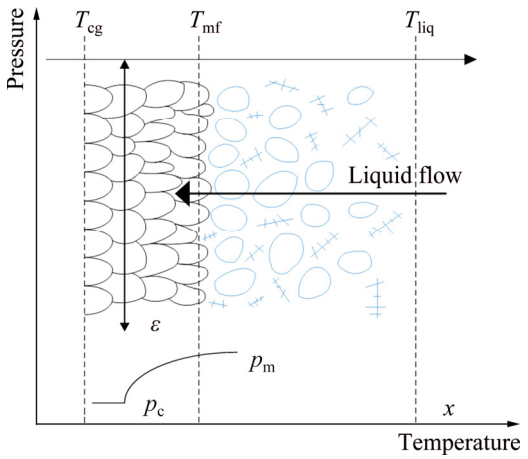

Fig. 17 Schematic diagram of equiaxed dendritic growth in inoculated aluminum alloys

4.3 Comparison of criterion

In Tables 2 and 3, mechanical-based criterion and non-mechanical-based criterion of hot cracking are listed, respectively. Differences and theoretical basis among these criteria can be seen clearly from these two tables. According to Refs. [9,21], only the Suyitno's criterion is used for casting practically. Suyitno's criterion gives a precise prediction of whether a hot tear will form under given solid fraction and strain rate. However, the parameters required are unavailable and not easy to get from current technology. Clyne and Davies's and Kou's criteria have easier access to the parameters provided for the calculation. All parameters needed are easily calculated from thermodynamic software. Therefore, these two criteria can be used to predict the HTS successfully. The limitation of these two criteria is that they cannot predict whether a hot tear will form accurately. Thus, the selection of a proper criterion for experiment depends on the complexity of required parameters. The RDG criterion takes both solidification shrinkage and deformation induced fluid flow into account. This criterion is different from other empirical formulas because the

Table 2 Mechanical-based criterion of hot cracking

Criterion	Formula	Theoretical basis
Critical stress-based criterion	$\rho_i=\frac{4\gamma}{3h}\left(1+\varepsilon\left(\frac{f_s^m}{1-f_s^m}\right)\right)^{-1}$	Induced stress > critical strength of body
Critical strain-based criterion	$\varepsilon_{\theta\theta}/\varepsilon_{fr}$	Critical strain > fracture strain
Critical strain rate-based criterion	$\dot{\varepsilon}_{max}=\frac{G^2\lambda_2^2}{180(1+\beta)B\mu\Delta T_0^2}\Delta p_{max}-\frac{V_T G\beta A}{(1+\beta)B\Delta T_0}$	Maximum strain rate that the mushy zone can sustain

Table 3 Non-mechanical-based criterion of hot cracking

Criterion	Formula	Theoretical basis
Clyne and Davies's criterion	$\mathrm{CSC}=\frac{t_v}{t_R}=\frac{t_{0.99}-t_{0.9}}{t_{0.9}-t_{0.4}}$	Considering critical time spent during solidification
Suyitno's criterion [21]	$\mathrm{HSC}=\frac{a_{crit}}{a}=\frac{4r_s E/(\pi\sigma^2)}{C_1 d}$	Combining critical liquid feeding theory, deformation rate and cavity formation
Kou's criterion [20]	$\left\{\begin{array}{l}\frac{\mathrm{d}\varepsilon_{local}}{\mathrm{d}T}>\sqrt{1-\beta}\frac{\mathrm{d}\sqrt{f_s}}{\mathrm{d}T}+\\ \frac{1}{(\mathrm{d}T/\mathrm{d}t)}\frac{\mathrm{d}}{\mathrm{d}z}\left[\left(1-\sqrt{1-\beta}\right)\sqrt{f_s}v_z\right]\end{array}\right\}\sqrt{f_s}\to 1$	When net expansion exceeds liquid feeding

model is based on physics. However, the RDG criterion does not involve the expansion of hot cracking. Therefore, a new hot cracking criterion is still in need.

5 Conclusions

(1) Based on critical diameter method, the hot cracking tendency of 7075 semi-solid alloy under different conditions was studied by combining experiment and simulation. The results show that the dendrite arms of the rod grow from the edge to the center. The smaller the diameter of the rod is, the more obvious the directional growth of dendrite is, and the greater the tendency of hot cracking is.

(2) Compared with common melt of 7075 alloy, the semi-solid technology can reduce the tendency of hot cracking effectively at some extent. With the decrease of mould temperature and pouring temperature, the effective plastic strain and the tendency of hot cracking decrease. For semisolid slurry, increasing mould temperature or decreasing pouring temperature can significantly improve hot cracking tendency of 7075 alloy, from 256 to 100 mm^2. Compared to the slender and fully developed dendrite cast structure, it is helpful to improve the tendency of hot cracking in solidification process.

(3) The RDG hot cracking criterion is applied to evaluating the hot cracking tendency. The results show that the cooling rate, the effective strain and the hot cracking tendency of the fine rod are larger than those of coarse rod. The hot cracking tendency decreases with the increase of mould temperature and the decrease of pouring temperature. The RDG criterion analysis results are consistent with the experimental results, which can be applied to the analysis of hot cracking tendency of specific parts. In addition, several hot cracking criteria are compared and discussed.

Acknowledgments

The authors would like to appreciate Shanghai Institute of Technology for providing software support.

References

[1] LIU B, PENG C Q, WANG R C, WANG X F, LI T T. Recent development and prospects for giant plane aluminum alloys [J]. The Chinese Journal of Nonferrous Metals, 2010, 20(9): 1705−1715. (in Chinese)

[2] WILLIAMS J C, STARKE E A. Progress in structural materials for aerospace systems [J]. Acta Materialia, 2003, 51: 5775−5799.

[3] WANG W Y, PAN Q L, WANG X D, SUN Y W, LONG L, HUANG Z Q. Mechanical properties and microstructure evolution of ultra-high strength Al−Zn−Mg−Cu alloy

processed by room temperature ECAP with post aging [J]. Materials Science and Engineering A, 2018, 731: 195−208.
[4] ZHANG X M, MAO W M, ZHU W Z. Influence of Zn, Mg and Cu contents on hot cracking behavior and microstructure of 7075 aluminum alloys [J]. Special Casting & Nonferrous Alloys, 2014, 34(12): 1336−1339.
[5] COLLEY L J, WELLS M A, MAIJER D M. Tensile properties of as-cast aluminum alloy AA5182 close to the solidus temperature [J]. Materials Science and Engineering A, 2004, 386: 140−148.
[6] van HAAFTEN W M, KOOL W H, KATGERMAN L. Tensile behaviour of semi-solid industrial aluminium alloys AA3104 and AA5182 [J]. Materials Science and Engineering A, 2002, 336: 1−6.
[7] ZALOŽNIK M, ŠARLER B. Modeling of macrosegregation in direct-chill casting of aluminum alloys: Estimating the influence of casting parameters [J]. Materials Science and Engineering A, 2005, 413−414: 85−91.
[8] SONG J, PAN F, JIANG B, ATRENS A, ZHANG M X, LU Y. A review on hot cracking of magnesium alloys [J]. Journal of Magnesium Alloy, 2016, 4: 151−172.
[9] ESKIN D G, SUYITNO K L. Mechanical properties in the semi-solid state and hot cracking of aluminium alloys [J]. Progress in Materials Science, 2004, 49: 629−711.
[10] TAGHIABADI R, FAYEGH A, PAKBIN A, NAZARI M, GHONCHEH M H. Quality index and hot cracking susceptibility of Al−7Si−0.35Mg−*x*Cu alloys [J]. Transactions of Nonferrous Metals Society of China, 2018, 28(7): 1275−1286.
[11] WANG Z, ZHOU Y, LI Y Z, WAG F, LIU Z, MAO P L, JIANG X P. Hot cracking behaviors and in-situ thermal analysis of Mg−7Zn−*x*Cu−0.6Zr alloys [J]. Transactions of Nonferrous Metals Society of China, 2018, 28(8): 1504−1513.
[12] JANAKIRAM G D, MITRA T K, SHANKAR V. Microstructural refinement through inoculation of type 7020 Al−Zn−Mg alloy welds and its effect on hot cracking and tensile properties [J]. Journal of Materials Processing Technology, 2003, 142: 172−181.
[13] KIMURA R, HATAYAMA H, SHINOZAKI K. Effect of grain refiner and grain size on the susceptibility of Al−Mg die casting alloy to cracking during solidification [J]. Journal of Materials Processing Technology, 2009, 209: 210−219.
[14] ZHOU B, KANG Y L, ZHU G M, GAO J Z, QI M F. Forced convection rheoforming process for semisolid slurry preparation and numerical simulation of 7075 aluminum alloy [J]. Transactions of Nonferrous Metals Society of China, 2014, 24(4): 1109−1116.
[15] ZHOU B, KANG Y L, GAO J Z, QI M F, ZHANG H H. Preparation of semisolid aluminum alloy slurry by forced convection mixing and its microstructure evolution [J]. The Chinese Journal of Nonferrous Metals, 2014, 24(1): 61−68. (in Chinese)
[16] SUYITNO, ESKIN D G, KATGERMAN L. Structure observations related to hot cracking of Al−Cu billets produced by direct-chill casting [J]. Materials Science and Engineering A, 2006, 420: 1−7.
[17] RAPPAZ M, DREZET J M, GREMAUD M. A new hot-cracking criterion [J]. Metallurgical and Materials Transactions A, 1999, 30: 449−455.
[18] AKHYAR H, MALAU V, SUYITNO, ISWANTO P T. Hot cracking susceptibility of aluminum alloys using CRCM-horizontal mold [J]. Results in Physics, 2017, 7: 1030−1039.
[19] BIRRU A K, KARUNAKAR D B. Effects of grain refinement and residual elements on hot cracking of A713 aluminium cast alloy [J]. Transactions of Nonferrous Metals Society of China, 2016, 26: 1783−1790.
[20] KOU S. A criterion for cracking during solidification [J]. Acta Materialia, 2015, 88: 366−374.
[21] SUYITNO, KOOL W H, KATGERMAN L. Integrated approach for prediction of hot tearing [J]. Metallurgical and Materials Transactioins A, 2009, 40: 2388−2400.
[22] BÖLLINGHAUS T, HEROLD H, CROSS C, LIPPOLD J C. Hot cracking phenomena in welds (II) [M]. Heidelberg: Springer, 2008: 1−466.
[23] CONIGLIO N, CROSS C E. Mechanisms for solidification crack initiation and growth in aluminum welding [J]. Metallurgical and Materials Transactions A, 2009, 40: 2718−2728.

7075 半固态铝合金的热裂实验与模拟

周 冰，陆 帅，徐凯乐，徐 春，王占勇，王斌君

上海应用技术大学 材料科学与工程学院，上海 201418

摘 要：基于临界直径法研究 7075 半固态铝合金在不同条件下的热裂敏感性。实验和模拟结果表明，枝晶臂倾向于由边缘向中心生长，试棒尺寸越小，枝晶臂的定向生长越明显，热裂倾向越大。与普通熔体相比，对于半固态浆料，提高模具温度或降低浇注温度可显著降低 7075 合金的热裂倾向，其热裂等级从 256 mm^2 降至 100 mm^2。此外，基于 RDG 准则并结合数值模拟，分析凝固条件对热裂倾向的影响，讨论 RDG 准则的应用和发展。

关键词：热裂倾向；半固态浆料；7075 铝合金；RDG 准则；数值模拟

(Edited by Wei-ping CHEN)